Supplementary Information to "The molecular structure of the surface of water-ethanol mixtures"

Johannes Kirschner,[a] Anderson H. A. Gomes,[b,1] Ricardo R. T. Marinho,[c] Olle Björneholm,[d] Hans Ågren,[d,e] Vincenzo Carravetta,[f] Niklas Ottosson,[g,2] Arnaldo Naves de Brito[b] and Huib J. Bakker[a]*

[a]Ultrafast Spectroscopy, AMOLF, 1098 XG Science Park, Amsterdam, The Netherlands

[b]Dept. of Applied Physics, Institute of Physics "Gleb Wataghin", University of Campinas, CEP: 13083-859 Campinas-SP, Brazil

[c] Institute of Physics, Federal University of Bahia, 40.170-115, Salvador, BA, Brazil

[d] Department of Physics and Astronomy, Uppsala University, 752 36 Uppsala, Sweden

[e] Theoretical Chemistry and Biology, School of Chemistry, Biotechnology and Health, KTH Royal Institute of Technology, SE-10044 Stockholm, Sweden

[f] CNR-IPCF, Institute of Chemical and Physical Processes, via G.Moruzzi 1, I-56124 Pisa, Italy

[g] EUV Photoemission, ARCNL, 1098 XG Science Park, Amsterdam, The Netherlands

[1] Current address: Laboratório Nacionalde Luz Síncrotron (LNLS)",13084-971 Campinas-SP, Brazil
[2] Current address: Swedish Research Council, Västra Järnvägsgatan 3, 111 64 Stockholm

Fitting Procedure

a) b)

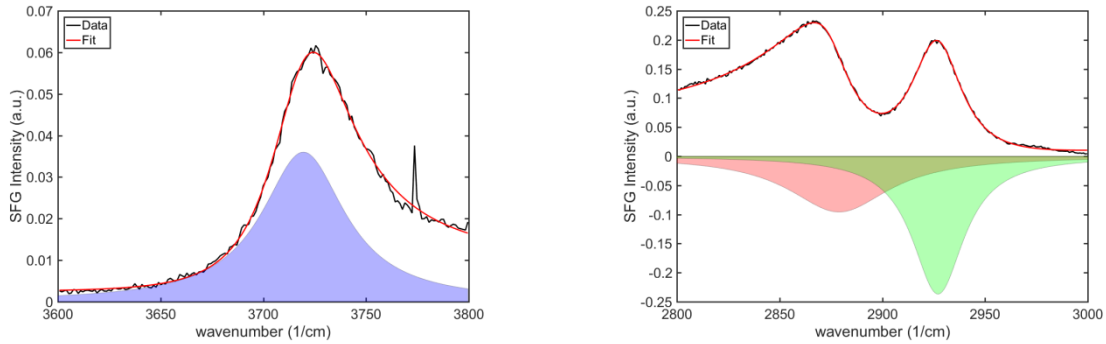

Figure S1: Fitting results of a) the free OH peak of pure H2O and b) the CH peaks of pure ethanol (SSP polarisation)

All spectra in this work were fitted using the equation

$$\chi^{(2)}(\omega_{IR}) = \chi_{NR}^{(2)} + \chi_R^{(2)} = A_{NR}e^{i\varphi} + \sum_n \frac{A_n}{(\omega_{IR} - \omega_n) + i\Gamma_n} \quad \text{(S 1)}$$

$\chi_{NR}^{(2)}$ and $\chi_R^{(2)}$ represent the non-resonant and resonant second order susceptibilities. The non-resonant part can be described by an amplitude and a phase difference to the resonant signal given by A_{NR} and φ, respectively. Each resonance of $\chi^{(2)}$ is described as a Lorentz function, with A_n, ω_n and Γ_n representing the amplitude, the centre frequency and the width of the n-th resonance. Depending on the orientation of the bond direction different signs of the peaks can result. This was taken into account by the free choice of the sign of the fit parameter A_n. Figure S1 shows the fit solutions in the two considered ranges (free OH and CH). Here the different choice of the peak orientation is visible.

a) b) c)

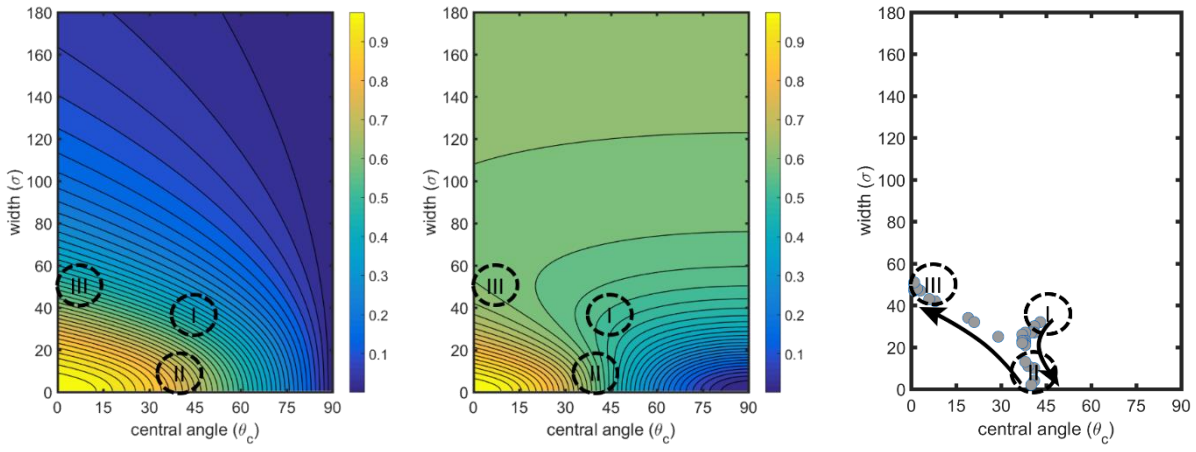

Figure S2: Dependence of a) ⟨cos(θ)⟩ and b) D on the central angle θ_c and the width of the angular distribution P(θ) as defined by equation (10) of the main manuscript, $P(\theta) = \sin(\theta)\, e^{-(\theta-\theta_C)^2/2\sigma^2}$. Panel c) shows the obtained values of the central angle θ_c and the width σ at the various studied ethanol concentrations (arrows indicate an increasing fraction of ethanol). The average orientational angle ⟨θ⟩ is given by $\int d\theta\, P(\theta)\, \theta$). It should be noted that the average orientational angle ⟨θ⟩ will differ from θ_c, especially when σ is large.

In Figure S2 a) and b) we present contour plots of ⟨cos(θ)⟩ and D that are calculated using the probability density function of equation (10) of the main manuscript, $P(\theta) = sin(\theta)\, e^{-(\theta-\theta_C)^2/2\sigma^2}$. The values of ⟨cos(θ)⟩ and D values thus directly follow from the values of the central angle θ_c and the width σ. Subsequently, we can use the experimentally determined ⟨cos(θ)⟩ and D value for each water-ethanol mixture to find the best fitting values of θ_c and the width σ, and thus the best fitting orientational distribution function P(θ). Figure S2 c) shows the obtained values for the central angle θ_c and the width σ for the studied water-ethanol mixtures. The resulting P(θ) for each composition can then be used to calculate the average angle ⟨θ⟩ (=∫dθ P(θ) θ) and the width of the orientational distribution, as defined as the full-width-at-half-maximum of P(θ). These are shown in Figure 10 of the main manuscript. In Figure S3 we show probability density functions $P(\theta) = sin(\theta)\, e^{-(\theta-\theta_C)^2/2\sigma^2}$ that are representative for regions I, II and III.

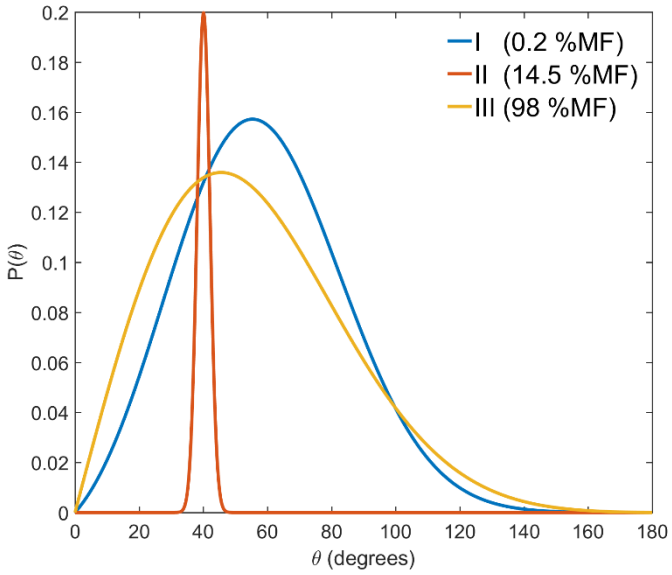

Figure S3: Orientational probability distribution function P(θ) for the three different regions indicated in Figure S2. The curves for region I and region III have been rescaled by a factor of 10 for better visibility.

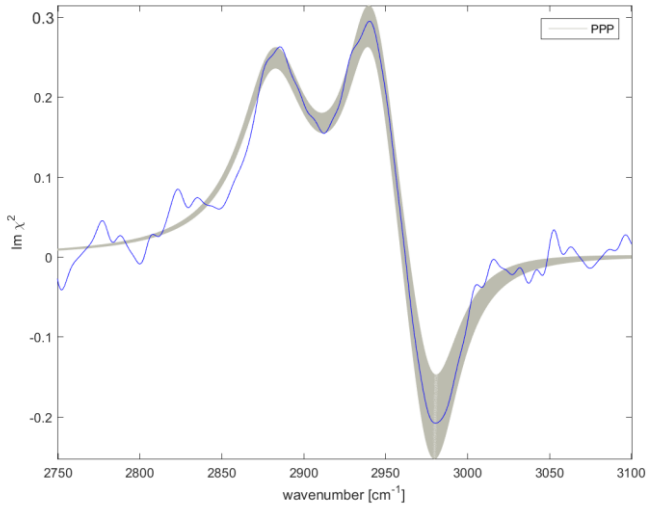

Figure S4: The fitted value of D from the VSFG spectra in PPP polarisation were varied ±0.05 (shown here as an exemplary for a concentration of 65%MF). Within these limits of D, the fits provided adequate results for all measured concentrations

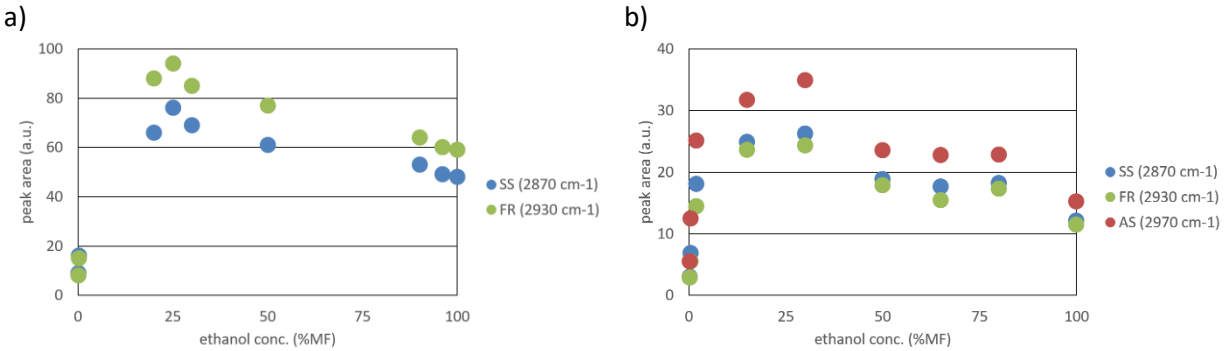

Figure S5: Peak areas of the detected CH vibrations using (a) the SSP and (b) the PPP polarization obtained from fitting.